Construction and Building Materials 408 (2023) 133740

Contents lists available at ScienceDirect

Construction and Building Materials

journal homepage: www.elsevier.com/locate/conbuildmat

Experimental investigation on axially-loaded threaded rods inserted perpendicular to grain into cross laminated timber

Osama Abdelfattah Hegeir *, Haris Stamatopoulos

Department of Structural Engineering, Norwegian University of Science and Technology (NTNU), Rich. Barcelonese 1A, 7491 Trondheim, Norway

ARTICLE INFO

Keywords:
Cross laminated timber (CLT)
Threaded rod
Self-tapping screws
Cyclic stiffness
Monotonic stiffness
Withdrawal stiffness
Withdrawal capacity
Pull-push loading configuration
Pull-pull loading configuration
Damping

ABSTRACT

This paper presents an experimental work on axially-loaded threaded rods inserted perpendicular to grain into the narrow face of cross laminated timber (CLT). Penetration length, loading type (tension, compression, fully reversed), and loading configuration (pull-pull and pull–push) were varied. The use of self-tapping screws as reinforcement was also explored. Stiffness under cyclic and monotonic loading, damping ratio, withdrawal capacity, failure mode, reinforcement effect, and influence of loading history were investigated. The experimental results highlight the high withdrawal stiffness and capacity of threaded rods embedded into CLT elements, and hence their effectiveness as fasteners for stiff timber connections.

1. Introduction

1.1. Background

The light weight and moderate stiffness of timber buildings limit the possibility for taller timber buildings. This is mainly due to increased wind-induced accelerations and lateral deformations under service-level loading [1–4]. The structural performance of timber structures relies heavily on their connections' properties [1–4]. Stiff connections can therefore be used to allow for taller timber buildings [4].

Connections with threaded rods (i.e. rods with wood screw threads and greater diameters than self-tapping screws, typically 16–22 mm) generally feature high withdrawal strength and stiffness [5–7]. Threaded rods can be used in timber structures as fasteners in moment resisting connections [8], axially loaded connections, or can be used as reinforcements [9]. Compared to glued-in rods (abbr. GiR), threaded rods are less prone to construction quality problems. Experimental work on GiR has shown that the presence of defects or sawdust in the pre-drilled holes can influence their behavior [10,11]. Compared to GiR, systems of rods screwed into wood exhibit better fire resistance [12], and they are less brittle [5,13]. Threaded rods can also be pre-installed allowing a high degree of pre-fabrication [8], reducing the work onsite. Moreover, threaded rods can be designed following capacity design principles to allow for ductile behavior (e.g. yielding in the steel rods) [5,7].

Using cross laminated timber (abbr. CLT) elements as lateral load resisting system is becoming popular [14–19] due to their high in-plane strength and stiffness and their availability in larger dimensions than standard glued laminated timber (abbr. glulam). CLT panels consist of sawn timber boards, glued together in alternating directions resulting in panels with high in-plane strength and stiffness and better dimensional stability [20]. Due to their high in-plane strength and stiffness, the performance of CLT panels depends highly on their connections [20].

The advantage of utilizing the high withdrawal strength of inclined self-tapping screws (abbr. STS) was first presented by Bejtka and Blaβ [21]. A predictive model based on the results of 387 withdrawal tests for STS inserted into the wide and narrow face of CLT was developed by Uibel and Blaβ [22]. Equations for the calculation of withdrawal capacity and strength of STS in softwood based on 1850 withdrawal tests were proposed by Frese and Blaβ [23]. Pirnbacher et al. [24] investigated the influence of several parameters on withdrawal strength of STS and proposed a calculation equation for the withdrawal strength. Subsequently, numerous studies have investigated the behavior of STS. This includes research on their withdrawal capacity [25–32], their stiffness properties [25,33], their use as reinforcement [9], their use in timber-to-timber joints [34] and in steel-to-timber joints [35], and force

* Corresponding author.
E-mail addresses: osama.a.s.a.hegeir@ntnu.no (O.A. Hegeir), haris.stamatopoulos@ntnu.no (H. Stamatopoulos).

https://doi.org/10.1016/j.conbuildmat.2023.133740
Received 7 July 2023; Received in revised form 7 September 2023; Accepted 8 October 2023

distribution along screws [36].

The behavior of GiR in glulam and CLT has also been investigated by several studies, addressing their withdrawal capacity [37–44], stiffness [37,39,44], behavior as a group [45,46], failure modes [38], durability [47], use for strengthening existing timber structures [48], behavior in beam-to-beam [49,50] and beam-to-column [51,52] moment connections, and the impact of construction methods and defects on their capacity [10,11,53].

On the contrary, little research has investigated the properties of threaded rods embedded in timber. The withdrawal capacity and stiffness of threaded rods were studied by Stamatopoulos and Malo [5–7] and Blaβ and Krüger [54]. However, these studies were only conducted on glulam. An experimental study was conducted by Yang et al. [55] to investigate the pull-out behavior of threaded rods in CLT elements using a wall-type loading setup. In their study [55], the penetration length, number of threaded rods, and the effect of using reinforcement were investigated. Only monotonic tension load was applied to the rods, and therefore, properties such as cyclic stiffness, energy dissipation, and equivalent viscous damping were not reported in [55]. Besides – and to the knowledge of the authors - experimental studies of threaded rods embedded in CLT, subjected to pure axial loading conditions are lacking in the literature.

1.2. Objective and scope

In the research presented, an experimental work was performed to investigate the behavior of steel threaded rods screwed into CLT elements. Five test series were carried out with a total of 23 test specimens. Out of the five series, three series were first tested under service-level cyclic loading followed by a monotonic tension load to failure, one series was tested only under monotonic tension load to failure, and the last series was tested only under monotonic compression load to failure.

The experimental work aimed to investigate the withdrawal capacity, stiffness under monotonic and cyclic loading, energy dissipation, failure modes, and the influence of STS as reinforcement. The penetration length, the loading type (tension, compression, fully reversed), and the loading configuration (pull–push, pull-pull) were varied. The scope of this paper is limited to threaded rods inserted perpendicular to grain into the narrow face of CLT elements made of softwood with a reference moisture content of approximately 12 %. Moreover, only short-term loading is considered, and therefore, issues such as long-term loading, moisture dependency, and fatigue are out of the scope of this work.

2. Materials and test methods

2.1. Materials

Fig. 1 depicts the CLT panel used in this study. Non-edge glued, three-layer CLT panels made of Norwegian spruce were used. The board thickness and width were 33 mm and 100 mm, respectively, and the total thickness was 100 mm, see Fig. 1. The outer layers and the inner layer were strength class T22 and T15, respectively (strength classes as defined by EN338 [56]). The CLT panels were stored in a climate room with controlled temperature and relative humidity of 20 °C and 65%, respectively. Prior to testing, the moisture content of each specimen was measured using an electric moisture meter and verified to be in the range of 10–12 %. The material properties of the used CLT panels are summarized in Table 1.

Table 1
Material properties of lamellae [57].

Strength class	$f_{m,k}$	$f_{t,0,k}$	$f_{c,0,k}$	$E_{0,mean}$	$E_{90,mean}$	ρ_k	ρ_{mean}
	N/mm^2					kg/m^3	
T15	22.0	15	21	11,500	380	360	430
T22	30.5	22	26	13,000	430	390	470

Fig. 2(a) shows the geometry of the threaded rod used in this study. The rod is of class 8.8 and consists of 110 mm metric thread and 440 mm wood thread. The metric thread is used for attaching the rod to the loading jack. The wood thread has a core diameter (d_1) of 16.1 mm, an outer thread diameter (d) of 22 mm, and a thread pitch of 8 mm. The rods were screwed into the narrow face of the CLT panels in pre-drilled holes with diameter equal to their core diameter (d_1), confer Fig. 2(b). The holes are drilled all the way through the test specimen.

In one of the test series, STS was used as reinforcement. STS with 100 mm length (equal to the thickness of the CLT elements) were not available at the time of testing. Instead, 160 mm-long screws were used, 60 mm longer than the thickness of the CLT. Since the actual embedded length of the screws is limited to the CLT panel thickness, the use of 160 mm-long is equivalent to the use of 100 mm-long screws. The screws have an outer thread diameter of 8 mm, an inner thread diameter of 5 mm, and a characteristic yield strength of 1000 N/mm^2 [58].

2.2. Loading and variation of penetration length

In this paper, two force levels were considered: service-level load and destructive load. The service-level load is taken to be 40 % of the capacity, as recommended by EN 12512 [59] to ensure elastic behavior. Prior to testing, the withdrawal capacity is unknown and therefore was estimated ($F_{ax,est}$) by use of a simplified equation proposed by Stamatopoulos and Malo [7]:

$$F_{ax,est} \approx 15 \cdot d \cdot l \cdot \left(\frac{\rho_{mean}}{470}\right) \quad (1)$$

where $F_{ax,est}$ is the estimated withdrawal capacity in N, d is the outer thread diameter of the rod in mm, l is the penetration length in mm, and ρ_{mean} is the mean density in kg/m^3.

Fig. 1. CLT panel.

To study the effect of the penetration length on the withdrawal stiffness, four penetration lengths were investigated: 5, 10, 15 and 20 times the outer thread diameter (5d, 10d, 15d, 20d), confer Fig. 3. The threaded rod is first screwed into the specimens at a 5d penetration length, and the service-level load testing is then performed. The same threaded rod is further screwed into the specimen at a step of 5d, and testing is performed again for 10d, 15d and 20d penetration lengths. At penetration lengths of 5d, 10d, 15d, and 20d, the rod fully penetrated one, two, three and four lamellae, respectively.

Monotonic loading does not represent various real-case loading scenarios such as wind or human excitation. To investigate stiffness and energy dissipation under such scenarios, cyclic load testing is more representative. Therefore, in this paper, two loading protocols were considered:

1. Service-level: Cyclic loading was applied for each penetration length shown in Fig. 3.
2. Destructive: Monotonic load is applied to failure, only at a 20d penetration length.

The loading protocols for service-level and destructive loading are shown in Fig. 4. Three test series were tested under service-level loading followed by destructive loading (in tension). Two test series were tested only under destructive loading, with one series tested in tension and the other in compression.

A simplified cyclic loading with constant amplitude was used in this paper, confer Fig. 4(a). Three types of cyclic loading were applied: cyclic tension (abbr. T), cyclic compression (abbr. C), and cyclic fully reversed (abbr. FR). The load limits for tension and compression cyclic loading were set to $0.10{\cdot}F_{ax,est} \leftrightarrow 0.40{\cdot}F_{ax,est}$ (the forces are negative for compression and positive for tension). The load limits for fully reversed cyclic loading were set to $-0.40{\cdot}F_{ax,est} \leftrightarrow +0.40{\cdot}F_{ax,est}$. For each type of cyclic loading (T, C, FR), eight cycles were applied. The load was applied with force control and a quasi-static loading rate of one minute per cycle for tension and compression and two minutes per cycle for fully reversed. The loading rate was chosen to achieve a reasonable test duration, while also maintaining quasi-static loading within the range of approximately 0.02 mm/*sec*-0.20 mm/*sec* [59]. The number of cycles was determined to allow for the examination of cyclic stiffness variation, if present, while still achieving a reasonable test duration.

Monotonic loading was applied until failure of the specimen to investigate the withdrawal capacity. Since the monotonic loading was applied after the cyclic loading tests were performed, only a penetration length of 20d could be tested. Hence, the influence of varying the penetration length on the withdrawal capacity was not investigated. The monotonic loading specified by EN 26891 [60] was adopted, see Fig. 4 (b).

2.3. Experimental setup

Two loading configurations were considered in this study, pull–push loading, and pull-pull loading, confer Figs. 5 and 6, respectively. In the pull–push loading (Fig. 5), the specimen was supported on two steel plates at the bottom and clamped using two steel rectangular hollow

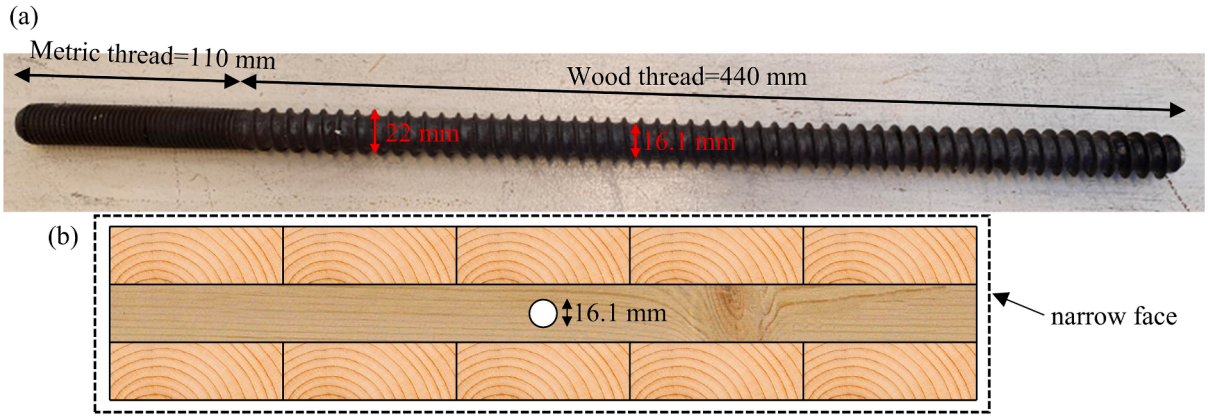

Fig. 2. (a) threaded rod, (b) predrilled hole at the narrow face of the CLT panel.

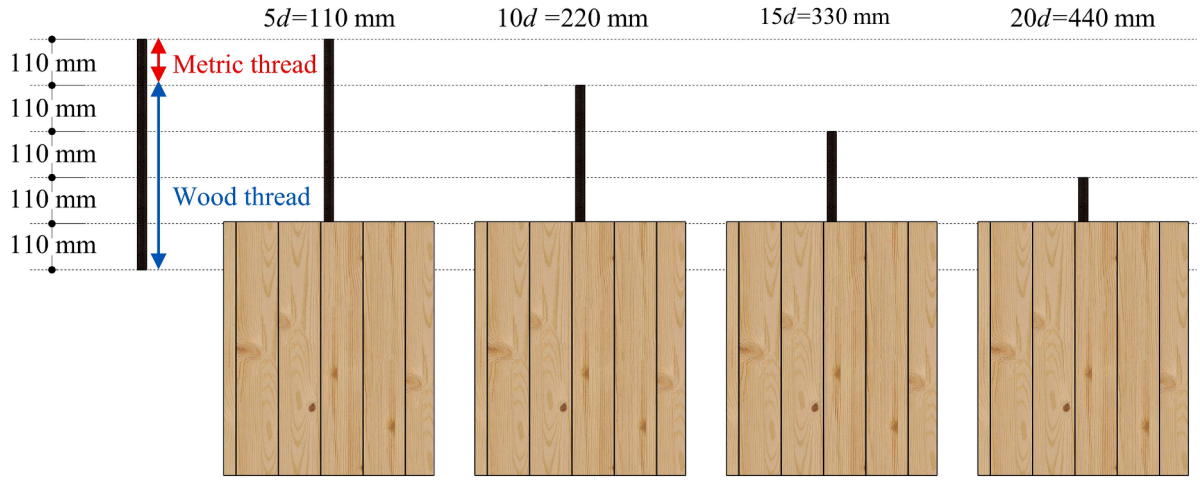

Fig. 3. Variation of penetration length.

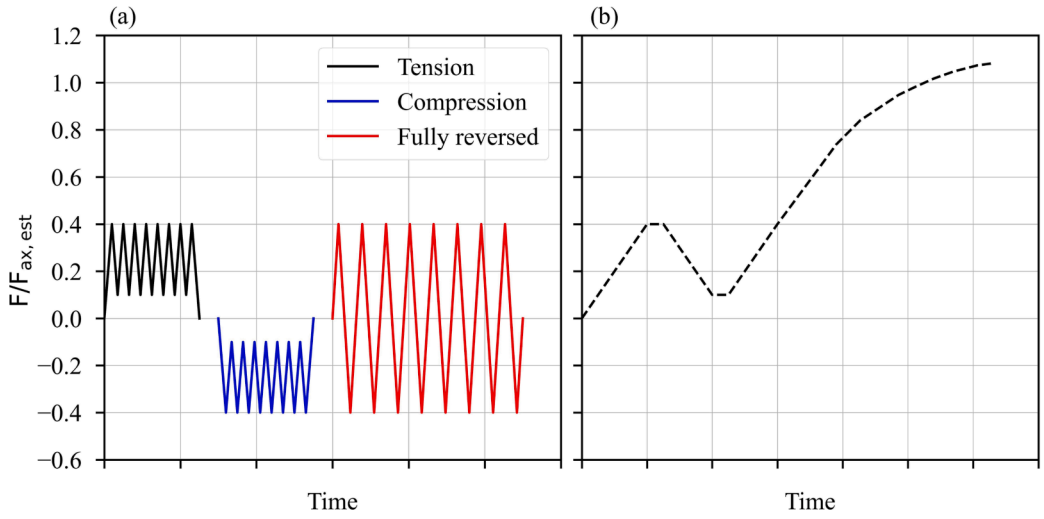

Fig. 4. Loading protocols (a) service level cyclic loading, (b) monotonic to failure loading.

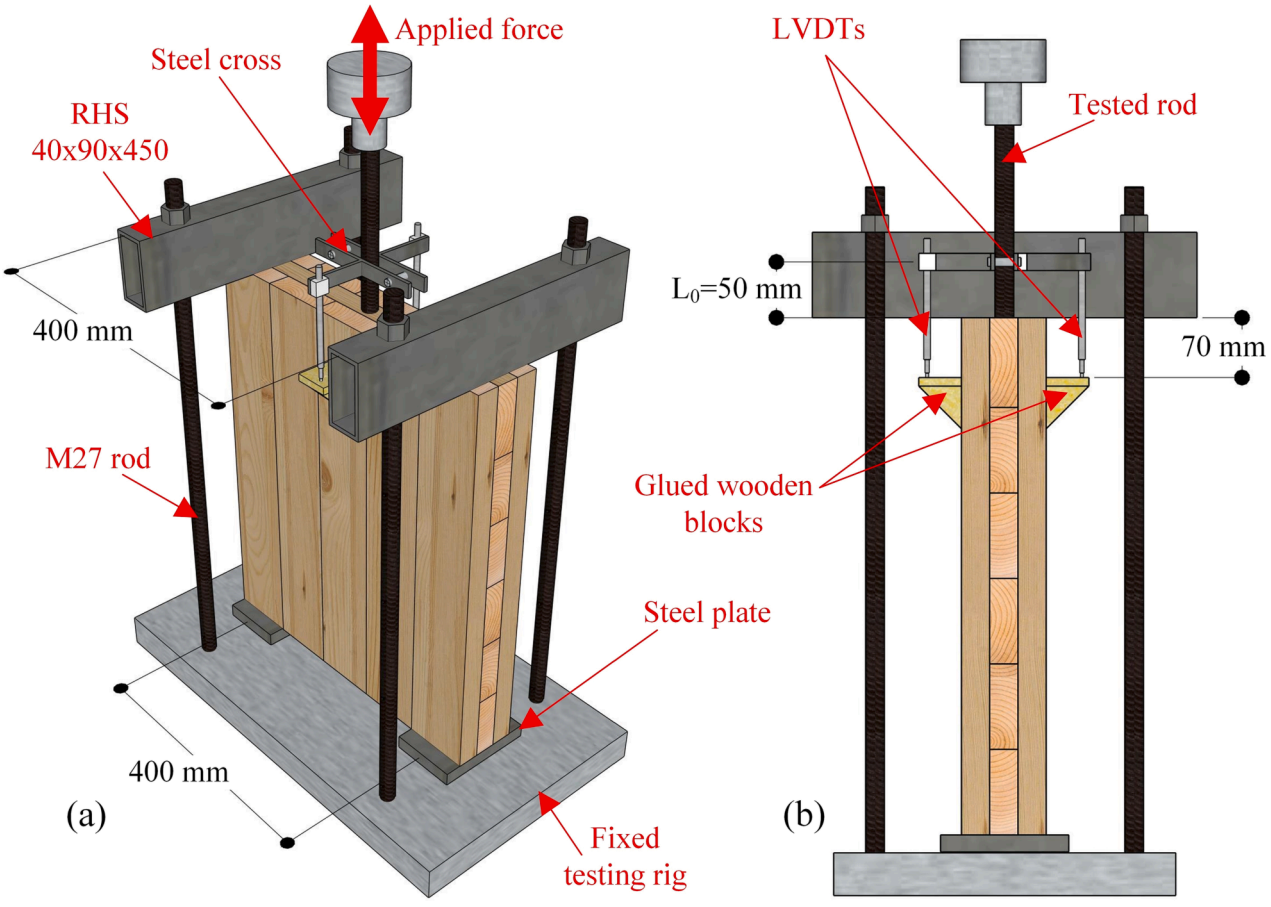

Fig. 5. Pull-push loading (a) 3D view, (b) side view.

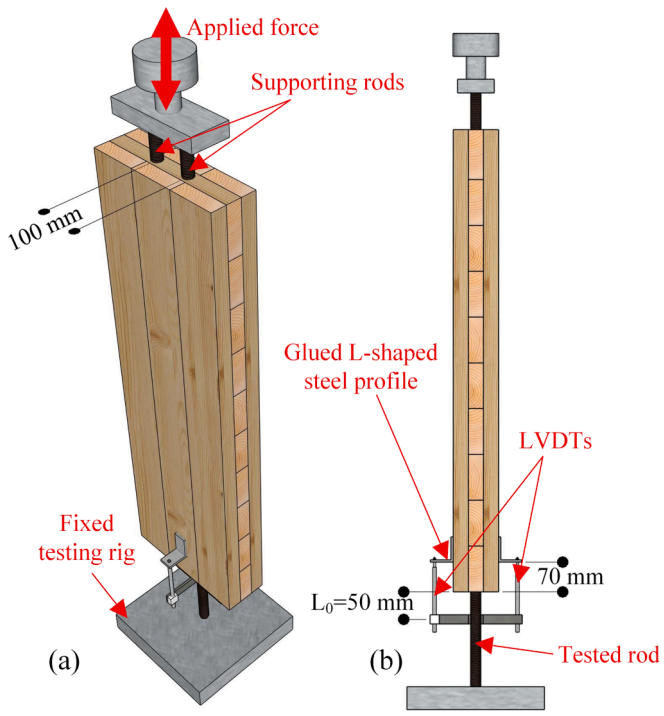

Fig. 6. Pull-pull loading (a) 3D view, (b) side view.

sections (abbr. RHS) at the top. In the pull-pull loading (Fig. 6), one rod (the tested rod) was inserted at one end of the specimen, and two rods were inserted at the other end. The use of two rods ensures the failure of the tested rod. For both loading configurations, linear variable differential transformers (abbr. LVDTs) were used to measure the displacements of the threaded rod relative to the test specimen, see in detail Figs. 5 and 6. Two wooden blocks or L-shaped steel profiles were glued at each side of the specimen to allow for measuring the relative displacement between the rod and the CLT specimen, confer Figs. 5 and 6. The average displacement of the two LVDTs was used as the withdrawal displacement. The LVDTs were attached to the rod using a purpose-made steel cross. The load was applied by attaching the metric part of the threaded rod to a loading jack. To facilitate the testing in pull-pull loading configuration, the specimens were rotated upside down (the tested rod is at the bottom) as shown in Fig. 6. To apply the load, the two rods at the top were connected to a rigid steel attachment and then

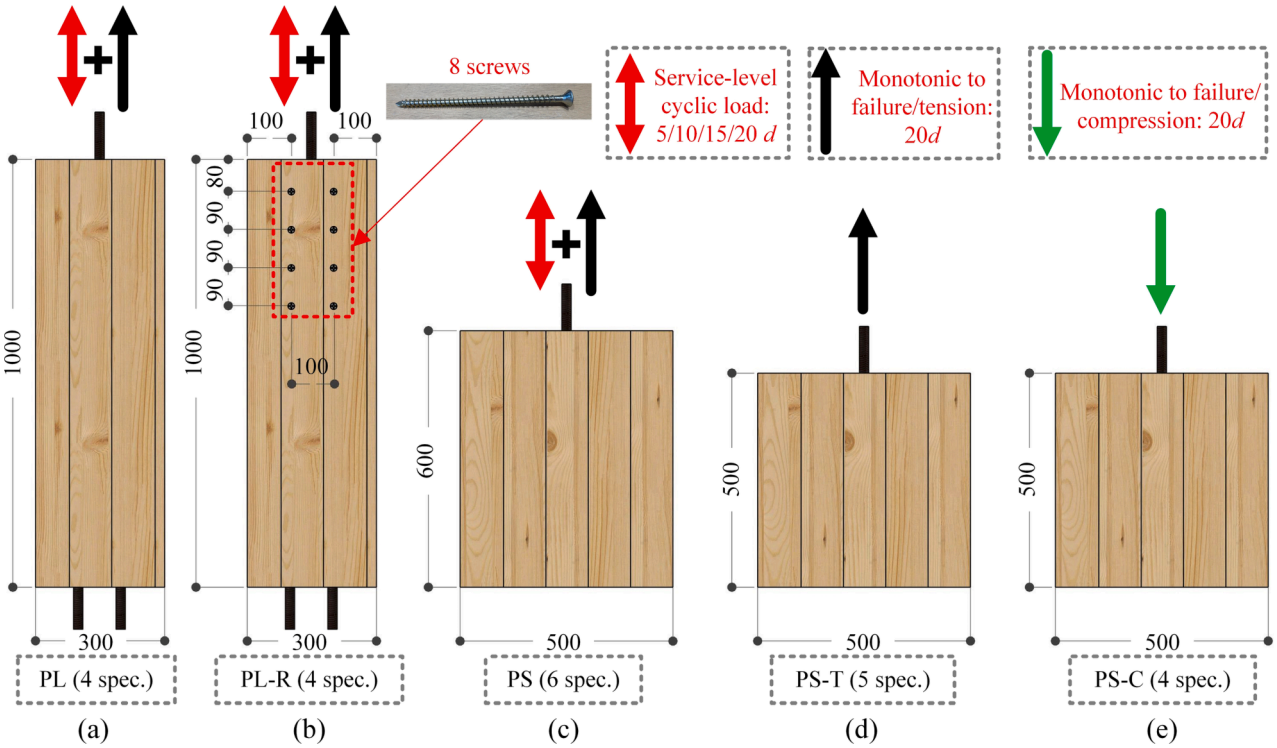

Fig. 7. Overview of test series (dimensions in mm).

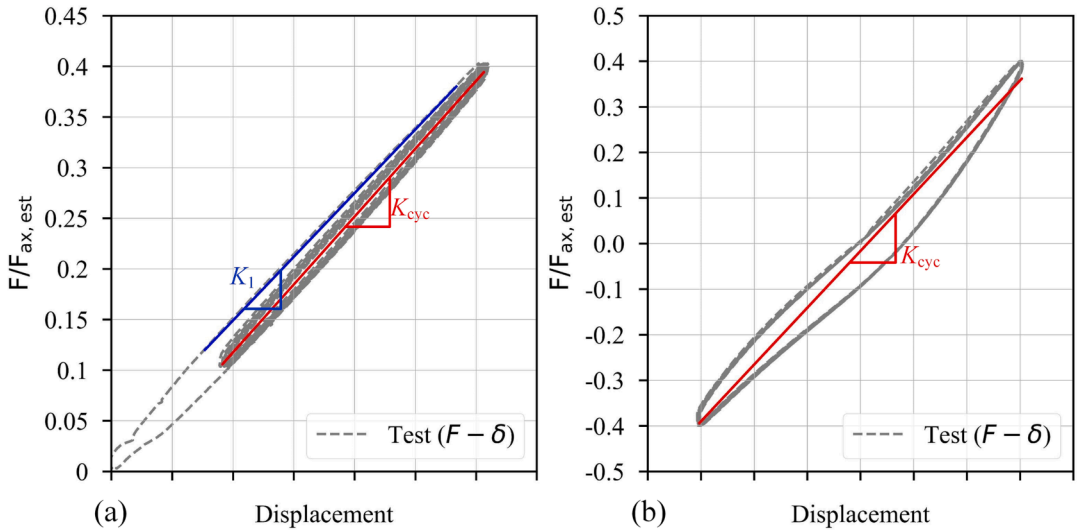

Fig. 8. Axial cyclic and monotonic stiffness (a) tension loading, (b) fully reversed loading.

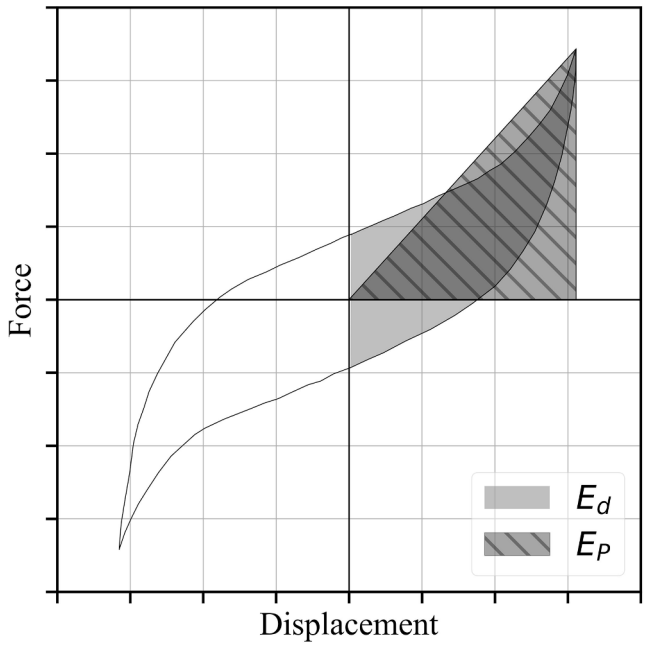

Fig. 9. Definition of dissipated and potential energy.

connected to a loading jack.

2.4. Test series

Fig. 7 illustrates all test series. In total, five experimental test series were conducted as follows:

1. PL (Fig. 7 (a)): Four specimens were tested in pull-pull loading (Fig. 6). The specimens were first subjected to service-level cyclic load at different penetration lengths, then tested to failure under monotonic tension at 20*d* penetration length.
2. PL-R (Fig. 7 (b)): Four specimens were tested in pull-pull loading (Fig. 6). The specimens had an identical geometry to PL, but were reinforced using eight STS. The specimens were first subjected to service-level cyclic load at different penetration lengths, then tested to failure under monotonic tension at 20*d* penetration length.
3. PS (Fig. 7 (c)): Six specimens were tested in pull–push loading (Fig. 5). The specimens were first subjected to service-level cyclic load at different penetration lengths, then tested to failure under monotonic tension at 20*d* penetration length.
4. PS-T (Fig. 7 (d)): Five specimens were tested in pull–push loading (Fig. 5). The specimens were tested to failure under monotonic tension at 20*d* penetration length.
5. PS-C (Fig. 7 (e)): Four specimens were tested in pull–push loading (Fig. 5). The specimens were tested to failure under monotonic compression at 20*d* penetration length.

Specimens tested in pull–push loading were prepared wider to allow for placing the supporting RHS beams on the top (Fig. 5). Specimens tested in pull-pull loading were prepared higher to accommodate the two supporting rods (Fig. 6). For both loading configurations, the number of vertical lamellae that were free to deform was approximately the same (three), confer Figs. 5–7.

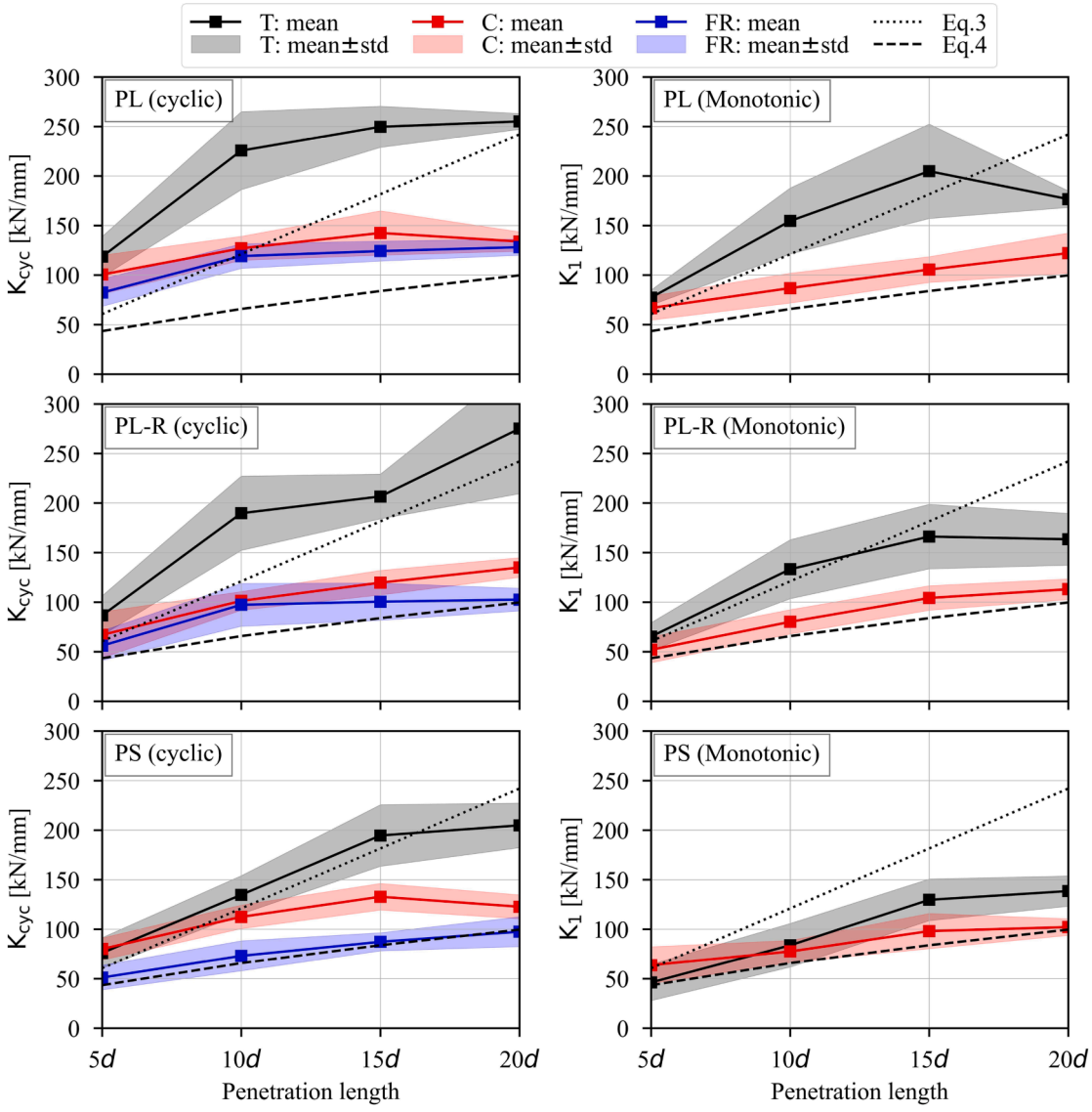

Fig. 10. Mean and standard deviation of cyclic and monotonic stiffness under cyclic loading.

Table 2
Mean and coefficient of variation (COV) of cyclic and monotonic stiffness under cyclic loading.

			Cyclic stiffness K_{cyc}**		Monotonic stiffness K_1**	
Test series	**Loading type**	**Penetration length**	**Mean (kN/mm)**	**COV (%)**	**Mean (kN/mm)**	**COV (%)**
PL	Cyclic tension	5*d*	118.4	17.2	77.2	9.8
		10*d*	225.5	17.5	154.5	21.5
		15*d*	249.7	8.3	204.7	23.3
		20*d*	255.1	3.1	176.5	4.7
	Cyclic compression	5*d*	100.4	19.5	66.6	18.2
		10*d*	126.9	9.5	86.8	17.3
		15*d*	142.4	15.7	105.5	12.3
		20*d*	133.8	7.3	122.1	16.6
	Cyclic fully reversed	5*d*	82.2	16.9	–	–
		10*d*	119.1	10.4	–	–
		15*d*	124.1	8.1	–	–
		20*d*	128.1	6.4	–	–
PL-R	Cyclic tension	5*d*	86.5	23.0	65.3	21.4
		10*d*	189.7	19.8	133.2	22.3
		15*d*	206.6	10.9	166.1	19.6
		20*d*	275.1	23.9	163.4	16.0
	Cyclic compression	5*d*	67.0	34.7	51.9	25.2
		10*d*	101.3	9.2	80.1	15.3
		15*d*	119.6	10.4	104.2	11.9
		20*d*	134.9	7.3	113.0	9.2
	Cyclic fully reversed	5*d*	56.0	26.7	–	–
		10*d*	97.3	22.2	–	–
		15*d*	100.4	18.7	–	–
		20*d*	102.6	11.1	–	–
PS*	Cyclic tension	5*d*	76.0	20.3	46.2	39.7
		10*d*	134.7	14.3	83.8	26.3
		15*d*	194.6	15.9	129.7	16.2
		20*d*	204.8	11.0	138.5	11.0
	Cyclic compression	5*d*	80.0	13.9	63.7	29.2
		10*d*	112.5	10.6	77.5	14.4
		15*d*	132.8	10.1	98.1	18.1
		20*d*	122.7	9.8	102.2	8.2
	Cyclic fully reversed	5*d*	51.1	24.3	–	–
		10*d*	73.1	20.8	–	–
		15*d*	87.3	10.5	–	–
		20*d*	97.5	15.4	–	–

*Result from one test specimen was considered as an outlier and was not included in the calculation, ** The reported values refer to the stiffness at the entrance point; the effect of the free length (L_0 = 50 mm) is removed considering the embedded part and the free length of the rod as springs in series.

2.5. Stiffness estimation

In the current version of Eurocode 5 [61], no formula is provided to calculate the axial stiffness of threaded rods in glulam or CLT. Under service-level cyclic loading (Fig. 4 (a)), two types of stiffness were estimated, the cyclic stiffness (K_{cyc}) and the monotonic stiffness (K_1), i.e. the stiffness at the first loading, confer Fig. 8.

The cyclic stiffness (K_{cyc}) was estimated by fitting a straight line (using the method of least squares) through each hysteresis loop of the cyclic test. The stiffness for each cycle was calculated individually, then the average value for all cycles was calculated and used as cyclic stiffness (K_{cyc}). The stiffness was calculated for all penetration lengths (5*d*, 10*d*, 15*d*, 20*d*), for cyclic tension, compression, and fully reversed loading ($K_{cyc,T}$, $K_{cyc,C}$, and $K_{cyc,FR}$).

The monotonic stiffness (K_1) was also estimated for all penetration lengths, for both cyclic tension and compression loading ($K_{1,T}$, $K_{1,C}$). According to EN 26891 [60], the stiffness is estimated from the monotonic loading protocol shown in Fig. 4 (b). The initial half cycle of the cyclic loading (from 0 to 40 % of $F_{ax,est}$) resembles the first loading ramp in the monotonic loading (from 0 to 40 % of $F_{ax,est}$). Therefore, the monotonic stiffness was estimated by fitting a line to the initial half cycle of the cyclic loading, see Fig. 8 (a). The stiffness under the monotonic loading shown in Fig. 4 (b) was also estimated by fitting a line to the first loading ramp from 10 % to 40 % of $F_{ax,est}$.

2.6. Equivalent viscous damping ratio

Under cyclic loading, several mechanisms contribute to energy dissipation. It is nearly impossible to describe such mechanisms mathematically [62]. It is therefore widely accepted to sum all energy dissipation mechanisms in an equivalent viscous damper [62]. The equivalent viscous damping ratio (ξ_{eq}) can be calculated as per EN 12512 [59]:

$$\xi_{eq} = \frac{1}{2\pi}\frac{E_d}{E_p} \tag{2}$$

where E_d is the energy dissipated per half cycle and E_p is the available potential energy, confer Fig. 9. The damping ratio for each cycle was calculated individually, then the average value across all cycles was calculated and used as the equivalent viscous damping ratio (ξ_{eq}). The equivalent viscous damping ratio (ξ_{eq}) is a non-dimensional parameter that represents the hysteresis damping of a joint. The damping ratio can be used for modeling the energy dissipation of members and connections under service-level cyclic loading using finite element analysis, see e.g. [8].

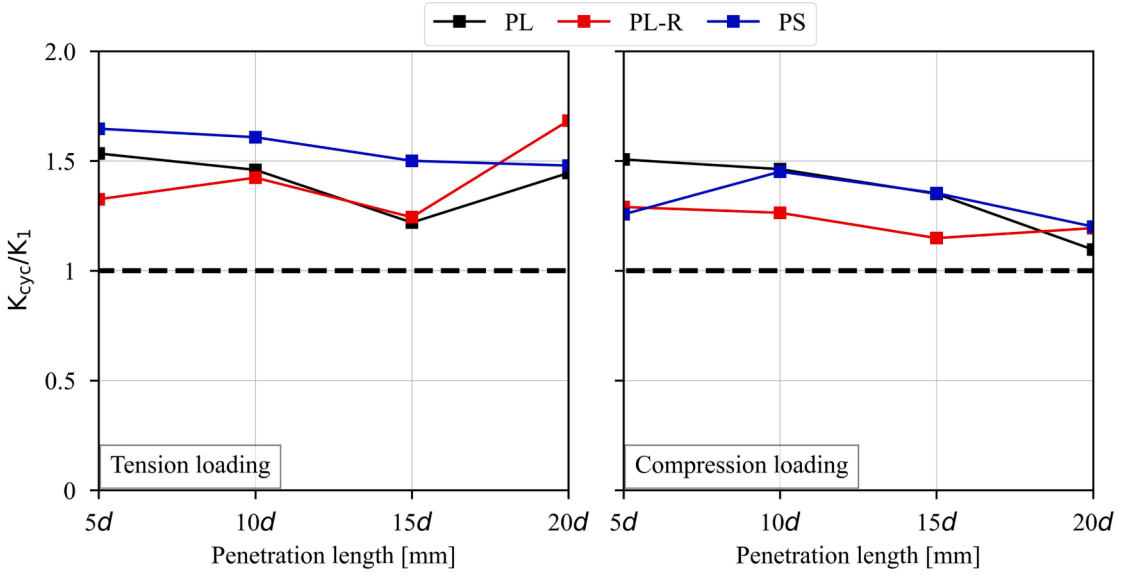

Fig. 11. Ratio of mean cyclic stiffness to mean monotonic stiffness.

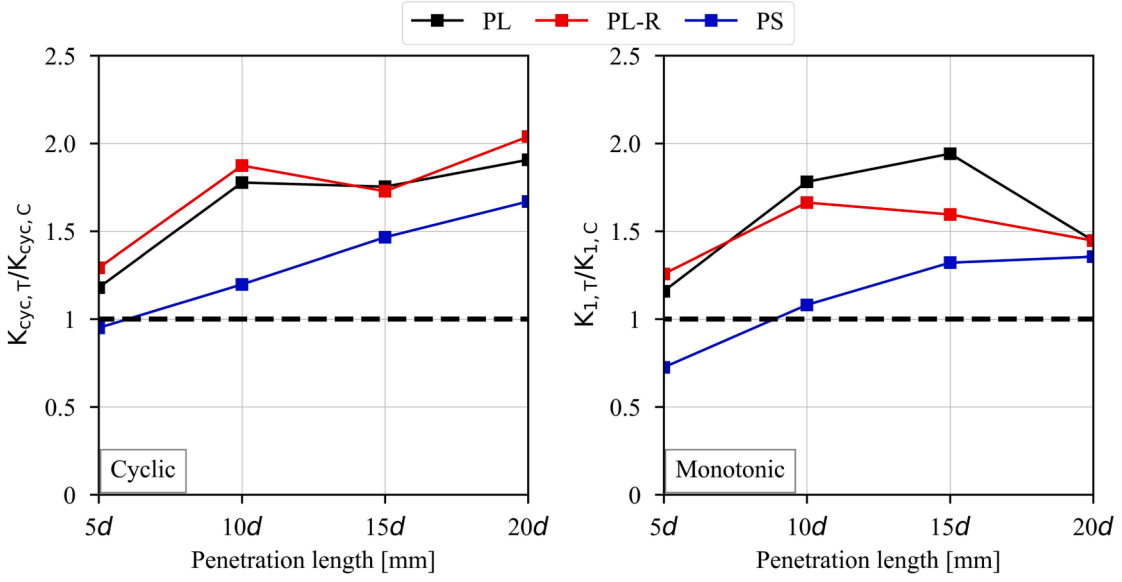

Fig. 12. Ratio of mean stiffness for tension to compression loading.

3. Experimental results and discussion

3.1. Service-level cyclic loading

3.1.1. Cyclic and monotonic stiffness

Fig. 8 (a) shows a representative force–displacement curve in tension at service-level cyclic loading, similar curves were observed for compression. Fig. 8 (b), shows a representative force–displacement curve under fully reversed service-level cyclic loading. As shown in this figure, little pinching (i.e. low stiffness around zero force) and immediate load-take up without initial slip was observed. As a result of the different stiffness in tension and compression (confer section 3.1.3), and the small pinching effect, the fitting of a line to the force–displacement curve under fully reversed loading has small deviation, confer Fig. 8 (b). However, it provides a fairly good fit to the experimental results. As shown in Fig. 8, the *F-δ* curves of all cycles coincide, and the stiffness estimated from all cycles was found to be nearly identical. Therefore, using the mean stiffness of all cycles provides an accurate approximation. Given the low load level and the observed identical *F-δ* curves for all cycles, it is likely that further loading cycles would exhibit a similar behavior.

Fig. 10 shows the cyclic and monotonic withdrawal stiffness of PL, PL-R, and PS test series, obtained from the cyclic load tests as function of penetration length. The results are also summarized in Table 2. The mean value is indicated by a solid line and the standard deviation (abbr. std) is indicated by a shaded area around the mean, confer Fig. 10. As shown in the figure, in general, both cyclic and monotonic stiffness (K_{cyc} and K_1) are higher for tension loading than for compression loading. This difference may be attributed to the different boundary conditions and different load paths under tension and compression loading. Claus et al. [36] performed withdrawal testing using innovative screws with internal fiber Bragg gratings to measure the forces along screws embedded in wood. The results in [36] show significant differences in the force distribution along the screw length under different boundary conditions. Experimental work by Ringhofer and Schickhofer [63] has shown that testing boundary conditions have no major influence on the

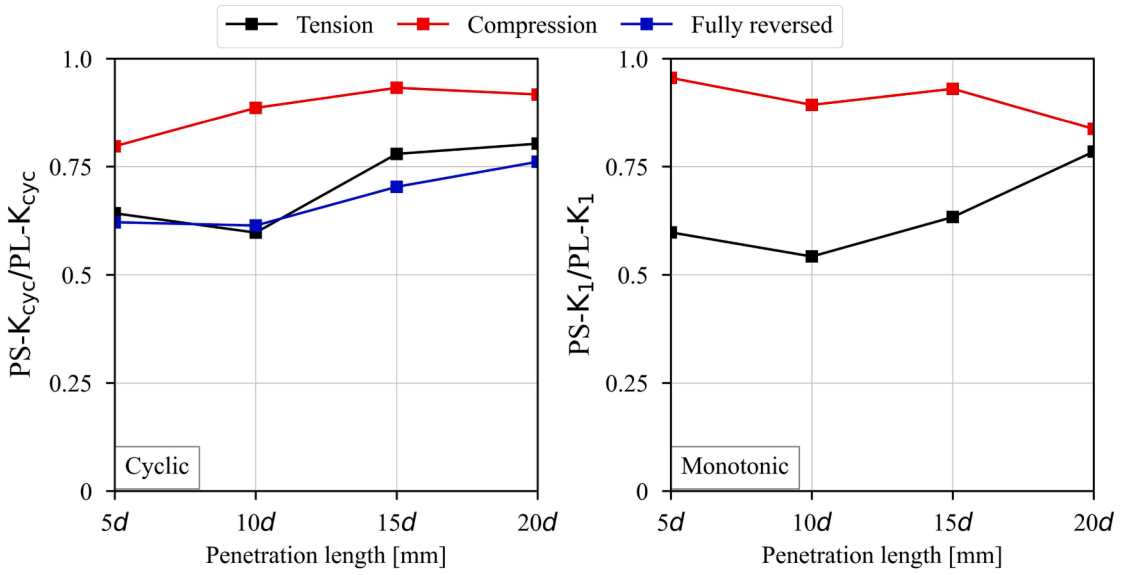

Fig. 13. Ratio of mean stiffness for pull-pull to pull–push loading.

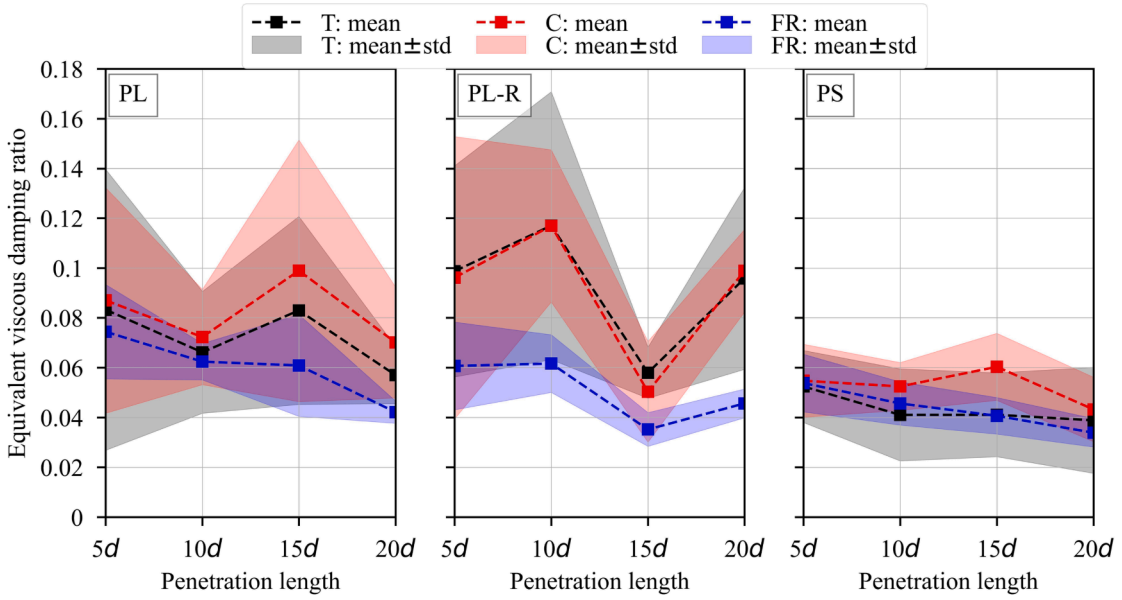

Fig. 14. Mean and standard deviation of equivalent viscous damping ratio.

withdrawal capacity of STS. However, studies on the influence of testing boundary conditions on the withdrawal stiffness of STS and threaded rods are lacking in literature.

As a result of small pinching effects, the fully reversed loading shows lowest stiffness compared to tension and compression loading. Both cyclic and monotonic stiffness exhibit a non-linear relationship with penetration length, showing noticeable convergence beyond 15*d* (330 mm) penetration length.

Several models for calculating the withdrawal stiffness $K_{SLS,ax}$ of STS and threaded rods are available in literature. Eq. (3) is commonly reported in several technical approvals. Despite the lack of guidelines for the estimation of the withdrawal stiffness of axially loaded fasteners in the current version of Eurocode 5 [61], the current draft for the next generation of Eurocode 5 [64] provides Eq. (4) for withdrawal stiffness of axially loaded screws and threaded rods.

$$K_{SLS,ax} = 25 \cdot d \cdot l \tag{3}$$

$$K_{SLS,ax} = 160 \cdot \left(\frac{\rho_{mean}}{420}\right)^{0.85} \cdot d^{0.9} \cdot l^{0.6} \tag{4}$$

In Eq. (3) and Eq. (4), $K_{SLS,ax}$ is in N/mm, d and l are in mm, and ρ_{mean} is in kg/m^3.

As shown in Fig. 10, Eq. (4) represents a lower bound for the cyclic and monotonic stiffness under tension, compression, and fully reversed loading. A better stiffness estimation can be obtained by use of Eq. (3). However, a limit on the penetration length should be set for Eq. (3) as the stiffness shows a noticeable convergence beyond 15*d* (330 mm) penetration length.

To evaluate the difference in displacements between the outer layers (measured by the LVDTs shown in Figs. 5 and 6) and the middle layer, two additional LVDTs were placed at the top of the test specimens of series PS. The stiffness estimated from these additional LVDTs at the top was found to be, on average, 5 % different from the stiffness estimated from the LVDTs placed at the sides, showing that deformations occur predominantly in the middle layer.

Fig. 15. Failure modes of all test series.

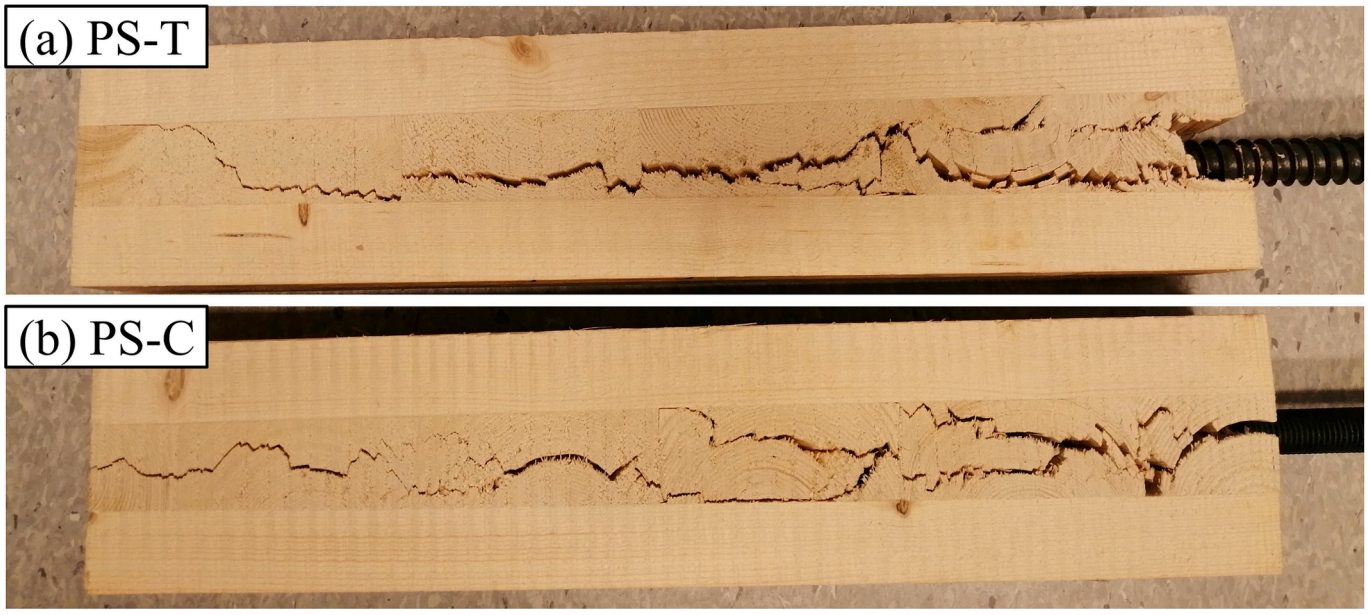

Fig. 16. Representative cut-open specimens.

3.1.2. Cyclic vs monotonic stiffness

Fig. 11 shows the ratio of the mean cyclic stiffness to the mean monotonic stiffness (K_{cyc}/K_1) under cyclic tension and compression. The cyclic stiffness is 10–68 % higher than the monotonic stiffness. On average, cyclic stiffness is 45 % and 30 % higher than monotonic stiffness for tension and compression loading, respectively.

3.1.3. Tension vs compression

The ratio of the mean cyclic stiffness under tension and compression loading ($K_{cyc,T}/K_{cyc,C}$) and the ratio of mean monotonic stiffness ($K_{1,T}/K_{1,C}$) are shown in Fig. 12. Apart from the PS series with 5*d* penetration length, stiffness values are higher for tension loading than compression loading.

3.1.4. Pull-pull vs pull–push

The mean cyclic and monotonic stiffness for PL series (pull-pull) and P*S* series (pull–push) were compared. Fig. 13 shows the ratio of mean cyclic stiffness (PS-K_{cyc}/PL-K_{cyc}) and mean monotonic stiffness (PS-K_1/PL-K_1). Mean stiffness of the pull–push series (PS) is lower compared to the pull-pull series (PL).

3.1.5. Equivalent viscous damping ratio

Fig. 14 shows the mean and standard deviation of the equivalent viscous damping ratio ξ_{eq} calculated according to Eq. (2). The mean damping ratio for all test series ranges from 0.03 to 0.12. In general, pull-pull loading (PL and PL-R) shows higher mean values and higher variability than pull–push loading (PS).

3.2. Monotonic to failure loading

The failure modes were visually inspected after each test. Fig. 15 shows the failure modes of representative specimens from the five test series. For PL series, the four specimens failed in a combined withdrawal and splitting failure, confer Fig. 15 (a). The PL-R, however, did not show splitting failure and only withdrawal failure was observed for all specimens, confer Fig. 15 (b). This suggests that the use of reinforcement can prevent splitting failure. For PS and PS-T series, all specimens failed in withdrawal failure mode, confer Fig. 15 (c) and (d). For PS-C series, under compression loading, the threaded rod pushed through the CLT specimen, and the thickness of the specimen increased around the location of the rod (*bulging*), confer Fig. 15 (e).

Representative specimens from test series PS-T and PS-C were cut open to examine their internal surface, confer Fig. 16. As shown in Fig. 16, the failure is accompanied by rolling shear failure and splitting perpendicular to grain in the middle layer. Despite this failure mode, high withdrawal capacity was attained in all tests. Failure accompanied by rolling shear failure has been reported for GiR [46] and screwed-in threaded rods [55] inserted perpendicular to grain into the narrow face of CLT elements.

Fig. 17 shows the monotonic load–displacement curves for all test series. The mean load–displacement ($F-\delta$) curves were calculated by fitting a higher degree polynomial to the test results. To ease the comparison between different test series, both tension and compression forces and the corresponding displacements are plotted positive.

Fig. 18 shows the mean load–displacement ($F-\delta$) curves for all test series. Comparing the PL (pull-pull, unreinforced) with the PL-R (pull-pull, reinforced), both have similar mean withdrawal capacity. However, the PL-R has better post failure load carrying capacity and shows more gradual drop in the load beyond failure. This suggests that using STS as reinforcement can enhance the post failure behavior without noticeable increase in withdrawal capacity. However, since only the rods at 20*d* penetration length were tested to failure, the effect of reinforcement using STS at different penetration lengths was not investigated. Experimental results of threaded rods embedded in CLT [55] shows that the effect of STS varies depending on the embedment length, with greater effect observed for shorter lengths.

Comparing the load–displacement curves (confer Figs. 17 and 18) of test series PS (with loading history) and PS-T (without loading history), small difference can be observed with PS-T showing lower stiffness and withdrawal capacity. However, the difference is small and therefore difficult to conclude whether this difference is attributed to loading history or natural variability of the tested material. The observed failure mode for all specimens of PS and PS-T series was withdrawal (confer Fig. 15 (c) and (d)), suggesting no influence of loading history on the failure mode. Among all test series tested in pull–push (PS, PS-T, and PS-C), the PS-C series shows the highest withdrawal capacity and lowest

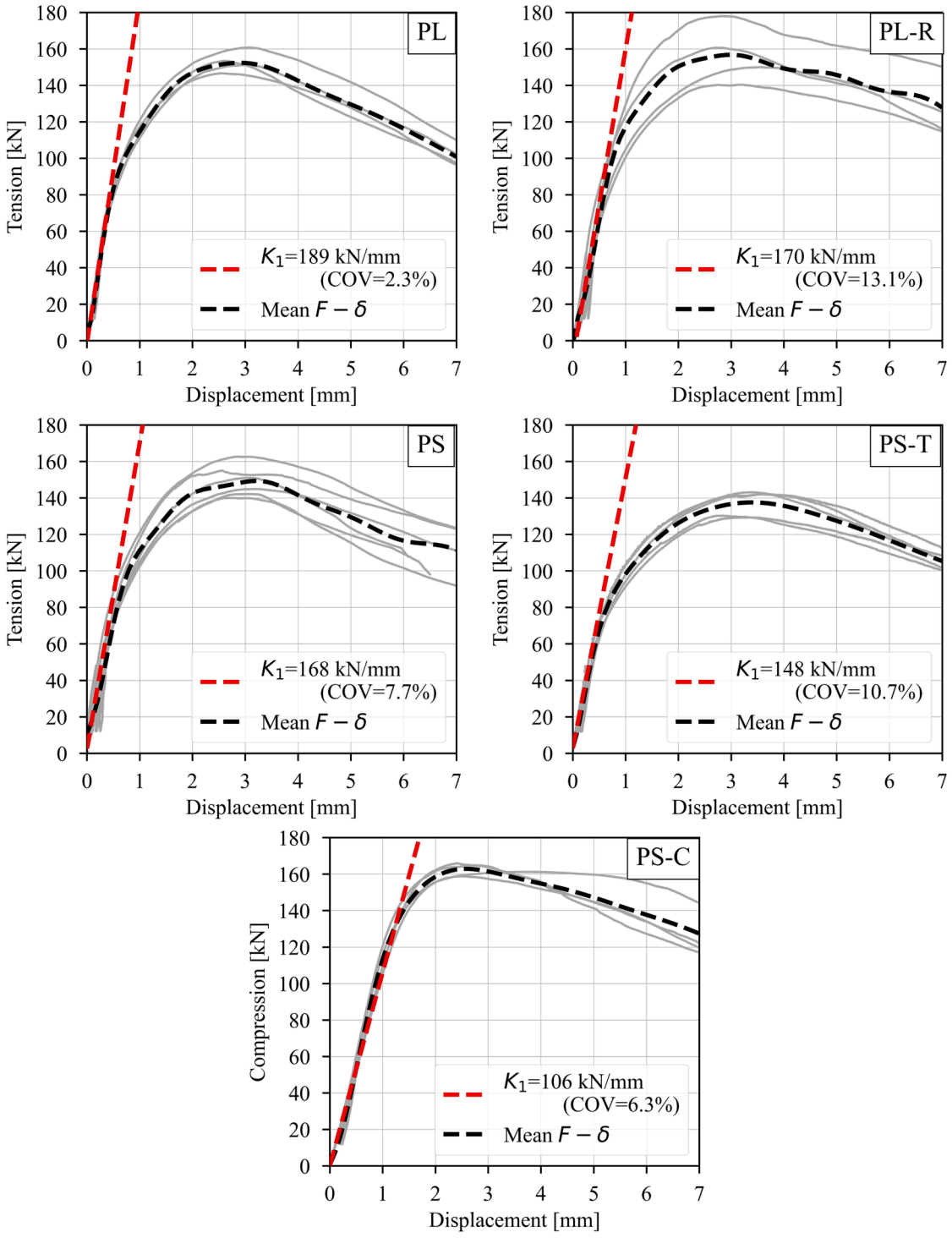

Fig. 17. Monotonic load–displacement curves.

monotonic stiffness, confer Figs. 17 and 18.

The mean withdrawal capacity ($F_{ax,mean}$) and mean withdrawal strength ($f_{ax,mean} = F_{ax,mean}/\pi dl$) at failure were calculated, see Table 3. The mean withdrawal capacity of all test series is comparable, with a difference of less than 20 % between different series. The characteristic withdrawal capacity $F_{ax,k}$ and the characteristic withdrawal strength ($f_{ax,k}$) were calculated according to EN 14358 [65] assuming lognormal distribution, see Table 3. Although test series PL-R shows higher mean withdrawal strength compared to PL, it has higher variability resulting in lower estimation for the characteristic withdrawal capacity.

Stamatopoulos and Malo [7] estimated mean withdrawal strength in the range of 4.46–5.12 N/mm^2 for threaded rods inserted perpendicular to grain in glulam. Blaβ and Krüger [54] reported mean withdrawal strength in the range of 3.72–4.68 N/mm^2 for similar rods inserted perpendicular to grain in softwood. Yang et al. [55] observed mean withdrawal strength in the range of 2.98–7.86 N/mm^2 for threaded rods inserted perpendicular to grain into the narrow face of CLT. Li et al. [30] reported mean withdrawal strength in the range of 4.76–8.10 N/mm^2 for STS inserted perpendicular to grain into the narrow face of CLT. The results shown in Table 3 agrees best with the values reported by

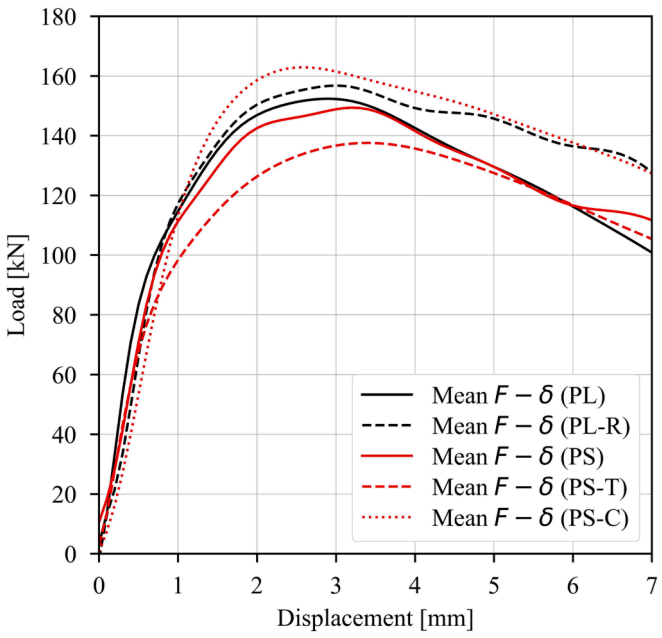

Fig. 18. Mean monotonic load–displacement curves.

Table 3
Mean and characteristic capacity and withdrawal stress.

Series	$F_{ax,mean}$ (kN)	$f_{ax,mean}$(N/mm^2)	$F_{ax,k}$ (kN)*	$f_{ax,k}$ (N/mm^2)*
PL	152.9 (COV = 3.8 %)	5.03	133.5	4.39
PL-R	157.2 (COV = 10.2 %)	5.17	119.0	3.91
PS	149.3 (COV = 5.8 %)	4.91	130.5	4.29
PS-T	137.3 (COV = 5.0 %)	4.52	120.9	3.98
PS-C	162.7 (COV = 2.0 %)	5.35	142.0	4.67

*Considering a minimum of 5% variability as specified by EN14358 [65].

Stamatopoulos and Malo [7] where threaded rods with similar diameter and wood of the same species were used.

4. Conclusions

This paper investigates the pullout behavior of threaded rods inserted perpendicular to grain into the narrow face of CLT elements. Threaded rods with outer thread diameter (d) of 22 mm were used in this study. Five test series were carried out, with three series tested under service-level cyclic loading followed by destructive monotonic loading, and two test series were tested under monotonic loading only. The influence of the penetration length, the loading type (tension, compression, fully reversed), the loading configuration (pull-pull, pull–push), and the effect of using self-tapping screws as reinforcement were investigated. The following main conclusions are drawn:

- Threaded rods inserted perpendicular to grain into the narrow face of CLT elements exhibit high withdrawal stiffness. When inserted at a penetration length of 20d, the mean withdrawal stiffness ranges from 100 to 250 kN/mm. The variation in the stiffness is possibly due to the different loading types and loading configurations.
- The mean withdrawal stiffness under cyclic loading is generally higher than the stiffness under monotonic loading.
- Under service-level loading, the equivalent viscous damping ratio ranges from 3 to 12 %.
- Stiffness exhibits a non-linear relationship with the penetration length, showing noticeable convergence beyond 15d (330 mm).
- Threaded rods inserted perpendicular to grain into the narrow face of CLT elements exhibit high withdrawal capacity. When inserted at a penetration length of 20 d, the mean withdrawal capacity ranges from 137 to 163 kN. The capacity seems not sensitive to the loading type and loading configuration.
- Reinforcement with self-tapping screws can provide more ductile load–displacement curve without noticeable increase in the withdrawal capacity. However, the effect of reinforcement at rod penetration lengths other than 20d was not investigated.
- All threaded rods with a penetration length of 20d failed in withdrawal failure mode. The only exception was for rods tested in pull-pull loading configuration without reinforcement where the withdrawal failure was combined with splitting failure. However, the influence of varying the penetration length on the failure mode was not investigated.

CRediT authorship contribution statement

Osama Abdelfattah Hegeir: Conceptualization, Methodology, Software, Validation, Formal analysis, Investigation, Data curation, Writing – original draft, Visualization, Project administration.

Declaration of Competing Interest

The authors declare that they have no known competing financial interests or personal relationships that could have appeared to influence the work reported in this paper.

Data availability

Data will be made available on request.

Acknowledgment

The authors acknowledge the contribution of Master Students Elisabeth Frette, Amund Heggheim, Thomas Munkeby, Haakon Flaten, Ulrik Sæther Langvik, and Simen Kåre Bokalrud in the preparation and execution of the experiments.

References

[1] A.S. Cao, H. Stamatopoulos, A theoretical study of the dynamic response of planar timber frames with semi-rigid moment-resisting connections subjected to wind loads, Eng. Struct. 240 (2021), https://doi.org/10.1016/j.engstruct.2021.112367.
[2] K.A. Malo, R.B. Abrahamsen, M.A. Bjertnæs, Some structural design issues of the 14-storey timber framed building "Treet" in Norway, Eur. J. Wood Wood Prod. 74 (3) (2016) 407–424, https://doi.org/10.1007/s00107-016-1022-5.
[3] A. Vilguts, H. Stamatopoulos, K.A. Malo, Parametric analyses and feasibility study of moment-resisting timber frames under service load, Eng. Struct. 228 (2021), https://doi.org/10.1016/j.engstruct.2020.111583.
[4] O. A. Hegeir, H. Stamatopoulos, and K.A. Malo, "Serviceability performance of timber dual frame-wall structural system under wind loading," World Conference on Timber Engineering (WCTE 2023), Oslo, Norway, 2023, doi: 10.52202/069179-0384.
[5] H. Stamatopoulos, K.A. Malo, Withdrawal capacity of threaded rods embedded in timber elements, Constr. Build. Mater. 94 (2015) 387–397, https://doi.org/10.1016/j.conbuildmat.2015.07.067.
[6] H. Stamatopoulos, K.A. Malo, Withdrawal stiffness of threaded rods embedded in timber elements, Constr. Build. Mater. 116 (2016) 263–272, https://doi.org/10.1016/j.conbuildmat.2016.04.144.
[7] H. Stamatopoulos, K.A. Malo, On strength and stiffness of screwed-in threaded rods embedded in softwood, Constr. Build. Mater. 261 (2020), https://doi.org/10.1016/j.conbuildmat.2020.119999.
[8] A. Vilguts, S.Ø. Nesheim, H. Stamatopoulos, K.A. Malo, A study on beam-to-column moment-resisting timber connections under service load, comparing full-scale connection testing and mock-up frame assembly, Eur. J. Wood Wood Prod. 80 (4) (2022) 753–770, https://doi.org/10.1007/s00107-021-01783-2.
[9] P. Dietsch, R. Brandner, Self-tapping screws and threaded rods as reinforcement for structural timber elements – a state-of-the-art report, Constr. Build. Mater. 97 (2015) 78–89, https://doi.org/10.1016/j.conbuildmat.2015.04.028.
[10] N. Ratsch, S. Böhm, M. Voß, M. Kaufmann, T. Vallée, Influence of imperfections on the load capacity and stiffness of glued-in rod connections, Constr. Build. Mater. 226 (2019) 200–211, https://doi.org/10.1016/j.conbuildmat.2019.07.278.

[11] D. Kohl, N. Ratsch, S. Böhm, M. Voß, M. Kaufmann, T. Vallée, Influence of manufacturing methods and imperfections on the load capacity of glued-in rods, J. Adhes. 96 (8) (2018) 738–759, https://doi.org/10.1080/00218464.2018.1508351.
[12] V. Di Maria, L. D'Andria, G. Muciaccia, A. Ianakiev, Influence of elevated temperature on glued-in steel rods for timber elements, Constr. Build. Mater. 147 (2017) 457–465.
[13] G. Tlustochowicz, E. Serrano, R. Steiger, State-of-the-art review on timber connections with glued-in steel rods, Mater. Struct. 44 (5) (2010) 997–1020, https://doi.org/10.1617/s11527-010-9682-9.
[14] M. Wells, "Stadthaus, London: raising the bar for timber buildings," in Proceedings of the Institution of Civil Engineers-Civil Engineering, 2011, vol. 164, no. 3: Thomas Telford Ltd, pp. 122-128.
[15] I. Gunawan et al., "Verification of seismic resistant performance of developed original cross-laminated timber core structure method by shaking table experiment," in IOP Conference Series: Materials Science and Engineering, 2020, vol. 935, no. 1: IOP Publishing, p. 012065.
[16] Z. Chen, M. Popovski, A. Iqbal, Structural performance of post-tensioned CLT shear walls with energy dissipators, J. Struct. Eng. 146 (4) (2020), 04020035.
[17] M. Shahnewaz, C. Dickof, T. Tannert, Seismic behavior of balloon frame CLT shear walls with different ledgers, J. Struct. Eng. 147 (9) (2021), 04021137.
[18] X. Sun, M. He, Z. Li, F. Lam, Seismic performance assessment of conventional CLT shear wall structures and post-tensioned CLT shear wall structures, Eng. Struct. 196 (2019), 109285.
[19] I. Gavric, M. Fragiacomo, A. Ceccotti, Cyclic behavior of CLT wall systems: experimental tests and analytical prediction models, J. Struct. Eng. 141 (11) (2015) pp, https://doi.org/10.1061/(asce)st.1943-541x.0001246.
[20] R. Brandner, G. Flatscher, A. Ringhofer, G. Schickhofer, A. Thiel, Cross laminated timber (CLT): overview and development, Eur. J. Wood Wood Prod. 74 (3) (2016) 331–351, https://doi.org/10.1007/s00107-015-0999-5.
[21] H. Blass, "Joints with inclined screws," CIB-W18, 2002. 9, 2002.
[22] T. Uibel and H. J. Blaß, "Edge joints with dowel type fasteners in cross laminated timber," in Proceedings. CIB-W18 Meeting, 2007.
[23] M. Frese and H. J. Blaß, "Models for the calculation of the withdrawal capacity of self-tapping screws," presented at the Proceedings of the 42nd CIB-W18 meeting Dübendorf, Switzerland, 2009.
[24] G. Pirnbacher, "Base parameters of self-tapping screws," in International Council for Research and Innovation in Building and Construction, Working Commission W18-Timber Structures, Meeting, 2009: . pp. 42-7-1/1-42-7-1/16.
[25] R. Tomasi, A. Crosatti, M. Piazza, Theoretical and experimental analysis of timber-to-timber joints connected with inclined screws, Constr. Build. Mater. 24 (9) (2010) 1560–1571, https://doi.org/10.1016/j.conbuildmat.2010.03.007.
[26] J. Xu, S. Zhang, G. Wu, Y. Gong, H. Ren, Withdrawal properties of self-tapping screws in Japanese larch (Larix kaempferi (Lamb.) Carr.) Cross Laminated Timber, Forests 12 (5) (2021) pp, https://doi.org/10.3390/f12050524.
[27] S. Maleki, S. Kazemi Najafi, G. Ebrahimi, M. Ghofrani, Withdrawal resistance of screws in structural composite lumber made of poplar (Populus deltoides), Constr. Build. Mater. 142 (2017) 499–505, https://doi.org/10.1016/j.conbuildmat.2017.03.039.
[28] A. Ringhofer, R. Brandner, G. Schickhofer, Withdrawal resistance of self-tapping screws in unidirectional and orthogonal layered timber products, Mater. Struct. 48 (5) (2013) 1435–1447, https://doi.org/10.1617/s11527-013-0244-9.
[29] M.P. Gutknecht, C. MacDougall, Withdrawal resistance of structural self-tapping screws parallel-to-grain in common Canadian timber species, Can. J. Civ. Eng. 46 (10) (2019) 952–962, https://doi.org/10.1139/cjce-2018-0374.
[30] X. Li, M. Ashraf, M. Subhani, K. Ghabraie, H. Li, and P. Kremer, "Withdrawal resistance of self-tapping screws inserted on the narrow face of cross laminated timber made from Radiata Pine," in Structures, 2021, vol. 31: Elsevier, pp. 1130-1140.
[31] J. Brown, M. Li, B. Karalus, and S. Stanton, "Withdrawal behaviour of self-tapping screws in New Zealand cross-laminated timber," 2020.
[32] A. Ringhofer, "Axially loaded self-tapping screws in solid timber and laminated timber products," 2017.
[33] N. Jacquier, U.A. Girhammar, Tests on glulam–CLT shear connections with double-sided punched metal plate fasteners and inclined screws, Constr. Build. Mater. 72 (2014) 444–457, https://doi.org/10.1016/j.conbuildmat.2014.08.095.
[34] C. Bedon, M. Fragiacomo, Numerical analysis of timber-to-timber joints and composite beams with inclined self-tapping screws, Compos. Struct. 207 (2019) 13–28.
[35] H. Krenn and G. Schickhofer, "Joints with inclined screws and steel plates as outer members," in International Council for Research and Innovation in Building and Construction, Working Commission W18-Timber Structures, Meeting, 2009: . pp. 42-7-2, 1-42-7-2, 12.
[36] T. Claus, W. Seim, J. Küllmer, Force distribution in self-tapping screws: experimental investigations with fibre Bragg grating measurement screws, Eur. J. Wood Wood Prod. 80 (1) (2021) 183–197, https://doi.org/10.1007/s00107-021-01740-z.
[37] B. Azinović, E. Serrano, M. Kramar, and T. Pazlar, "Experimental investigation of the axial strength of glued-in rods in cross laminated timber," Materials and Structures, vol. 51, no. 6, 2018, doi: 10.1617/s11527-018-1268-y.
[38] G.S. Ayansola, T. Tannert, T. Vallee, Experimental investigations of glued-in rod connections in CLT, Constr. Build. Mater. 324 (2022), https://doi.org/10.1016/j.conbuildmat.2022.126680.
[39] B. Azinović, H. Danielsson, E. Serrano, M. Kramar, Glued-in rods in cross laminated timber – numerical simulations and parametric studies, Constr. Build. Mater. 212 (2019) 431–441, https://doi.org/10.1016/j.conbuildmat.2019.03.331.
[40] R. Steiger, E. Gehri, R. Widmann, Pull-out strength of axially loaded steel rods bonded in glulam parallel to the grain, Mater. Struct. 40 (1) (2006) 69–78, https://doi.org/10.1617/s11527-006-9111-2.
[41] R. Widmann, R. Steiger, E. Gehri, Pull-out strength of axially loaded steel rods bonded in glulam perpendicular to the grain, Mater. Struct. 40 (8) (2007) 827–838, https://doi.org/10.1617/s11527-006-9214-9.
[42] D. Otero Chans, J. Estévez Cimadevila, E. Martín Gutiérrez, Withdrawal strength of threaded steel rods glued with epoxy in wood, Int. J. Adhes. Adhes. 44 (2013) 115–121, https://doi.org/10.1016/j.ijadhadh.2013.02.008.
[43] C. Grunwald, et al., Rods glued in engineered hardwood products part II: Numerical modelling and capacity prediction, Int. J. Adhes. Adhes. 90 (2019) 182–198, https://doi.org/10.1016/j.ijadhadh.2018.05.004.
[44] B.-H. Xu, D.-F. Li, Y.-H. Zhao, A. Bouchaïr, Load-carrying capacity of timber joints with multiple glued-in steel rods loaded parallel to grain, Eng. Struct. 225 (2020), 111302.
[45] E. Gonzalez, C. Avez, T. Tannert, Timber joints with multiple glued-in steel rods, J. Adhes. 92 (7–9) (2015) 635–651, https://doi.org/10.1080/00218464.2015.1099098.
[46] Y. Shirmohammadli, A. Hashemi, R. Masoudnia, P. Quenneville, Numerical modeling investigation of cross-laminated timber connections consisting of multiple glued-in rods, Structures 53 (2023) 491–500.
[47] E. Martín-Gutiérrez, J. Estévez-Cimadevila, D. Otero-Chans, Durability of joints made with threaded steel rods glued in chestnut timber – An experimental approach, Compos. B Eng. 108 (2017) 413–419, https://doi.org/10.1016/j.compositesb.2016.10.010.
[48] R. Steiger, et al., Strengthening of timber structures with glued-in rods, Constr. Build. Mater. 97 (2015) 90–105, https://doi.org/10.1016/j.conbuildmat.2015.03.097.
[49] N. Gattesco, A. Gubana, M. Buttazzi, M. Melotto, Experimental investigation on the behavior of glued-in rod joints in timber beams subjected to monotonic and cyclic loading, Eng. Struct. 147 (2017) 372–384.
[50] B.-H. Xu, A. Bouchaïr, P. Racher, Analytical study and finite element modelling of timber connections with glued-in rods in bending, Constr. Build. Mater. 34 (2012) 337–345.
[51] S. Navaratnam, J. Thamboo, T. Ponnampalam, S. Venkatesan, K.B. Chong, Mechanical performance of glued-in rod glulam beam to column moment connection: An experimental study, J. Build. Eng. 50 (2022), 104131.
[52] É. Gauthier-Turcotte, S. Ménard, M. Fiset, Strength and behavior of spruce pine glulam timber moment connections using glued-in steel rods, J. Struct. Eng. 148 (12) (2022), 04022192.
[53] E. Gonzales, T. Tannert, T. Vallee, The impact of defects on the capacity of timber joints with glued-in rods, Int. J. Adhes. Adhes. 65 (2016) 33–40, https://doi.org/10.1016/j.ijadhadh.2015.11.002.
[54] H.J. Blaß, O. Krüger, Schubverstärkung von Holz mit Holzschrauben und Gewindestangen, KIT Scientific Publishing, Karlsruhe, 2010.
[55] H. Yang, J. Ji, H. Tao, B. Shi, J. Hu, B. Wen, Pull-out behaviour of axially loaded screwed-in threaded rods embedded in CLT elements: experimental study, J. Renewable Mater. 10 (1) (2022) 105–117, https://doi.org/10.32604/jrm.2021.016118.
[56] CEN, "NS-EN 338: Structural timber–Strength classes," *European Committee for Standardization: Brussels, Belgium,* 2016.
[57] SINTEF Certification-TG 20712 Splitkon krysslimt tre, 2022.
[58] ETA-Danmark A/S, European Technical Assessment ETA-12/0114, SPAX self-tapping screws, 2017.
[59] CEN, "EN 12512: Timber structures-Test methods-Cyclic testing of joints made with mechanical fasteners," European Committee for Standardization: Brussels, Belgium, 2001.
[60] CEN, "EN 26891:1991 (ISO 6891:1983): Timber structures-Joints Made with Mechanical Fasteners- General Principles for the Determination of Strength and Deformation Characteristics," 1991.
[61] CEN, "NS-EN 1995-1-1:2004+A1:2008+NA:2010: Design of timber structures–Part 1-1: General–Common rules and rules for buildings," European Committee for Standardization: Brussels, Belgium, 2010.
[62] A.K. Chopra, *Dynamics of Structures*, fifth ed., Pearson Education Limited, London, United Kingdome, 2020.
[63] A. Ringhofer and G. Schickhofer, "Influencing parameters on the experimental determination of the withdrawal capacity of self-tapping screws," in Proceedings of the 13th World Conference on Timber Engineering. Canada, World Conference on Timber Engineering, 2014, vol. 2014, pp. 906-915.
[64] CEN/TC250/SC5N1650, " prEN 1995-1-1: Design of timber structures–Part 1-1: General rules and rules for buildings," European Committee for Standardization: Brussels, Belgium, 2022.
[65] CEN, "EN 14358:2016: Timber Structures: Calculation and verification of characteristic values," European Committee for Standardization: Brussels, Belgium, 2016.